PHYSICAL REVIEW D VOLUME 37, NUMBER 5 1 MARCH 1988

Heavy leptons at hadron supercolliders

V. Barger, T. Han, and J. Ohnemus
Physics Department, University of Wisconsin, Madison, Wisconsin 53706
(Received 13 July 1987; revised manuscript received 18 December 1987)

The production, decay, and detection of a fourth-generation charged heavy lepton L at multi-TeV hadron supercolliders is discussed for masses $m_L > M_W$ and $m_{\nu_L} \approx 0$. The leptonic and hadronic decay signals for single L production and $L\bar{L}$ pair production are evaluated. In all channels examined the heavy-lepton signal is smaller than backgrounds from single and pair production of $W^{\pm}$ and Z bosons. However, it may still be possible to detect a heavy lepton from its contribution to $\not{p}_T+2$ or 4 jets events where the $Z(\to\nu\bar{\nu})+$jets background may be determined from measurements of $(Z\to l\bar{l})+$jets events.

I. INTRODUCTION

One of the open questions in particle physics is the number of generations of quarks and leptons. Fourth-generation leptons could be produced at hadron colliders in the decays $W^+\to L^+\nu_L$ and $W^-\to L^-\bar{\nu}_L$ of real or virtual charged weak bosons. The best experimental signature[1,2] for $m_L < M_W$ and $m_{\nu_L}\approx 0$ arises from the decay $L\to\nu_L+$hadrons. Data from the UA1 Collaboration[3] on events with large missing transverse momentum and jets rule out the existence of a fourth-generation charged lepton with a mass less than 41 GeV, but only if ν_L is essentially massless.[4] The mass region $m_L \lesssim 60$ GeV should still be accessible at the CERN and Fermilab colliders.[2,5] The production rate for still heavier leptons at hadron colliders has also been evaluated.[6] It is of great interest to determine the feasibility of detecting heavy leptons that may be produced at proposed multi-TeV hadron colliders.

In this paper, the production, decay, and detection of a heavy charged lepton with mass $m_L > M_W$ is examined in detail for the Superconducting Super Collider (SSC) with a center-of-mass energy of 40 TeV. The new leptons are assumed to form a weak-isospin doublet with the same electroweak couplings as the first three generations of leptons. The neutrino ν_L associated with the heavy lepton is assumed to be massless. Both leptonic and hadronic decay modes for the heavy lepton are studied and compared to standard-model backgrounds. In all cases examined the heavy-lepton signal is smaller in all kinematic ranges than the backgrounds from single and pair production of $W^{\pm}$ and Z bosons. However, it may still be possible to detect a heavy lepton from its contribution to $\not{p}_T+2$ or 4 jets events where the $(Z\to\nu\bar{\nu})+$jets background may be determined from measurements of $(Z\to l\bar{l})+$jets events ($\not{p}_T$ denotes missing transverse momentum). Similar conclusions apply for the 17-TeV center-of-mass energy of the proposed CERN Large Hadron Collider (LHC).

Formidable backgrounds from heavy quarks are also expected at SSC and LHC energies since the gluon-fusion cross section for heavy-quark production rises faster with increasing center-of-mass energy than the cross section for heavy-lepton production.[5] Backgrounds from heavy-quark production and decay are not considered here since the other standard-model backgrounds already obscure the heavy lepton signal. Background contributions from non-standard-model processes may also exist; examples include supersymmetric, superstring, and technicolor particles. These non-standard-model backgrounds will not be considered here since their existence is uncertain.

The presentation of our results is organized as follows. The calculations are described in Sec. II. The results for five different heavy-lepton signals and their standard-model backgrounds are presented in Sec. III. Conclusions are given in Sec. IV. The matrix elements squared for the signals and backgrounds are given in Appendixes.

II. CALCULATIONS

The matrix elements of the subprocesses contributing to the heavy-lepton signals were evaluated at the parton level. The cross sections and distributions were then calculated by Monte Carlo techniques and were convoluted with the quark structure functions of Ref. 7, evolved in Q^2 up to $Q^2=\hat{s}$, where $\sqrt{\hat{s}}$ is the center-of-mass energy of the subprocess. Cross sections for single-weak-boson production, including single L and τ production, and Drell-Yan processes were multiplied by the order-α_s QCD correction factor[8]

$$K=1+\frac{16\pi^2}{9}\frac{\alpha_s(Q^2=\hat{s})}{2\pi}\ . \tag{1}$$

No K factors were included in the weak-boson pair production cross sections since they are not theoretically known. The background contributions from $pp\to Z+$QCD jets, with $Z\to\nu\bar{\nu}$ decay, and $pp\to W+$QCD jets, with $W\to e\nu$ decay, were calculated using the QCD shower model of Ref. 8 and were confirmed by ISAJET (Ref. 9) and PYTHIA (Ref. 10). Four generations of light neutrinos were assumed in the $Z\to\nu\bar{\nu}$ decay. The following electroweak parameters were used in all calculations: $x_W=0.23$, $M_W=80.6$ GeV,

$M_Z = 91.9$ GeV, and $\alpha(M_W) = \frac{1}{128}$.

In the case of hadronic L decay signals, the final-state quarks and gluons (the gluons occur in the initial-state radiation of the QCD shower-model calculations of the backgrounds) were regarded as potential jets. All final-state quarks and gluons were processed through an algorithm which parallels that of the UA1 experiment[11] for defining jets from hadrons (see Appendix B of Ref. 12 for details of the jet-defining algorithm used for partons). The jet-recognition threshold was taken to be $\sum |p_T| = E_T(\text{jet}) > 20$ GeV and the jet pseudorapidity y was required to satisfy $|y| < 5$. Distinct jets were required to have a separation in azimuth $\Delta\phi$ and pseudorapidity Δy that satisfy $(\Delta R)^2 = (\Delta\phi)^2 + (\Delta y)^2 > 0.5$. We assume that gluon jets cannot be distinguished from quark jets on an event by event basis.

III. SIGNALS

The dominant subprocesses for hadronic production of fourth-generation charged heavy leptons are illustrated in Fig. 1, with subsequent L decays. Since we are assuming $m_L > M_W$, the vector bosons in the L and $L\bar{L}$ production subprocesses are virtual. The expected cross sections at $\sqrt{s} = 40$ TeV are shown in Fig. 2 versus the L mass. Similar results have previously been given in Ref. 13. For the design luminosity of 10^4 events per year, these cross sections would yield substantial event rates. Henceforth, we concentrate on masses $m_L = 100$ and 200 GeV because of the larger signal at lower L masses, and neglect the gluon-fusion contribution, which becomes the dominant contribution at larger m_L. The following five heavy-lepton signals were examined and compared to their standard-model backgrounds.

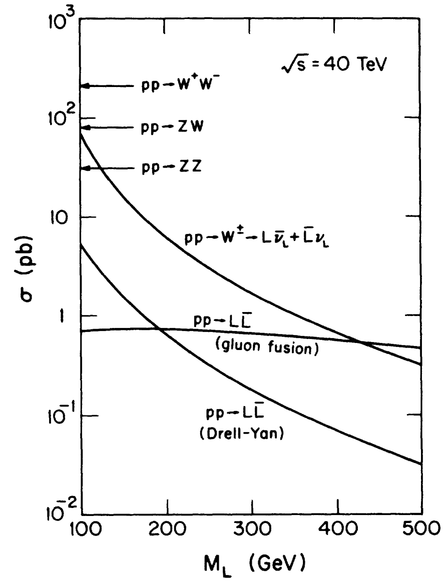

FIG. 2. Cross section for heavy-lepton production vs heavy-lepton mass. Production mechanisms shown are $pp \to W^\pm \to L\bar{\nu}_L + \bar{L}\nu_L$, $pp \to L\bar{L}$ (gluon-fusion), and $pp \to L\bar{L}$ (Drell-Yan). For the gluon-fusion curve, a Higgs-boson mass of $M_H = 100$ GeV and fourth-generation quark masses $M_v = M_L$ and $M_a = M_v + 250$ GeV are assumed. Cross sections for weak-boson pair production are indicated by arrows along the left-hand side of the figure.

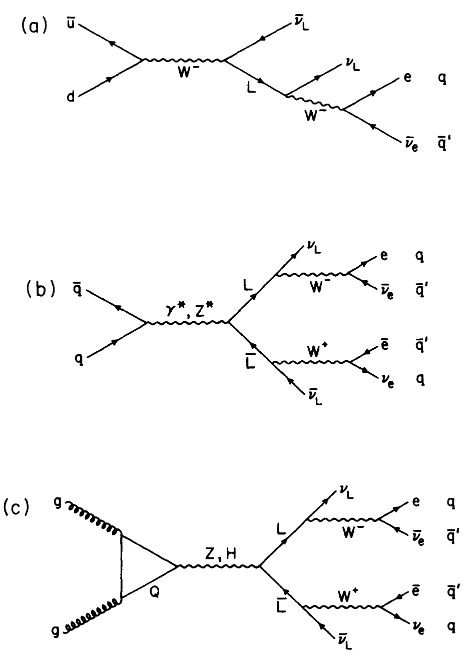

FIG. 1. Feynman diagrams for heavy-lepton production and decay: (a) L production $d\bar{u} \to W^- \to L\bar{\nu}_L$ with subsequent decay of L, (b) $L\bar{L}$ production $q\bar{q} \to \gamma^*, Z^* \to L\bar{L}$ with subsequent decays of L and $\bar{L}$, and (c) $L\bar{L}$ production by the gluon fusion via a virtual quark loop and an intermediate Z or Higgs boson with subsequent decays of L and $\bar{L}$.

(1) Single L production with leptonic decay, $L \to \nu_L e \bar{\nu}_e$ or $L \to \nu_L \mu \bar{\nu}_\mu$; see Fig. 1(a).

(2) Single L production with hadronic decays, $L \to \nu_L d\bar{u}$, $L \to \nu_L s\bar{c}$, or $L \to \nu_L b\bar{t}$ (we neglect the quark masses in our calculations).

(3) $L\bar{L}$ production via the Drell-Yan process, with leptonic decay of both L and $\bar{L}$; see Fig. 1(b).

(4) $L\bar{L}$ pair production via the Drell-Yan process, with leptonic decay of one heavy lepton and hadronic decay of the other heavy lepton.

(5) $L\bar{L}$ pair production via the Drell-Yan process, with hadronic decay of both L and $\bar{L}$.

Backgrounds to the above processes come from single W, Z production and W^+W^-, ZZ, WZ pair production and decay. The Feynman diagrams for the gauge-boson pair processes are shown in Fig. 3. The matrix elements squared for the Feynman diagrams in Figs. 1 and 3 are given in Appendixes B–F. Weak-boson pair production can alternatively be evaluated numerically using the helicity amplitude formalism of Ref. 14. The magnitudes of the gauge-boson pair contributions, which give rise to backgrounds to the L signal, are shown along the left side of Fig. 2.

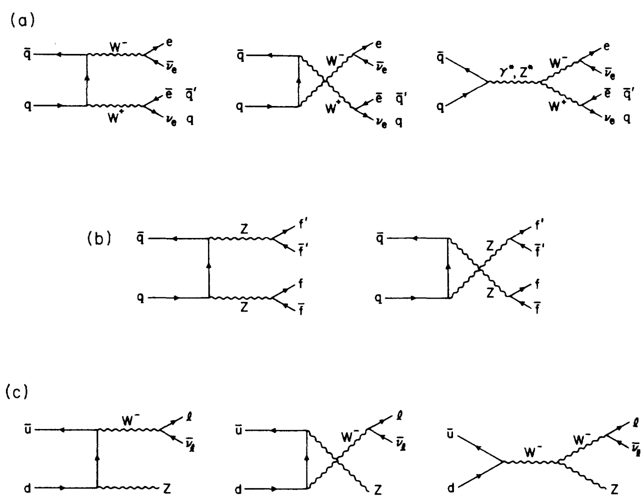

FIG. 3. Feynman diagrams for gauge-boson pair production and decay: (a) $q\bar{q}\to W^+W^-$ with subsequent decays $W^-\to e\bar{\nu}_e$ and $W^+\to\bar{e}\nu_e$ or $\bar{q}'q$ [the left (middle) diagram applies only to incoming quarks whose third component of weak-isospin is $T_3=+\frac{1}{2}$ ($T_3=-\frac{1}{2}$); the diagram on the right applies to both $T_3=\pm\frac{1}{2}$ quarks]; (b) $q\bar{q}\to ZZ$ with subsequent decays $Z\to f\bar{f}$ and $Z\to f'\bar{f}'$ where f and f' are fermions, and (c) $d\bar{u}\to W^-Z$ with subsequent decay $W^-\to l\bar{\nu}_l$, where $l=e$ or μ.

A. Leptonic decay of *L*

For single-*L* production and decay via the subprocess

$$d\bar{u}\to W^-\to L\bar{\nu}_L \qquad \hookrightarrow \nu_L W^-\to\nu_L e\bar{\nu}_e \tag{2}$$

the signature is a high-p_T electron or positron balanced by $\not{p}_T$. (The signature could also be $\mu^\pm$ and $\not{p}_T$.) (All transverse quantities are defined with respect to the beam axis.) Three standard-model processes which have the same signature as the signal are

$$pp\to W^-\to e\bar{\nu}_e\ , \tag{3}$$

$$pp\to W^-\to\tau\bar{\nu}_\tau\ , \qquad \hookrightarrow \nu_\tau e\bar{\nu}_e \tag{4}$$

$$pp\to W^-Z\ . \qquad Z\hookrightarrow \nu\bar{\nu}, \quad W^-\hookrightarrow e\bar{\nu}_e \tag{5}$$

The subprocess for Eq. (4) is exactly analogous to the L production and decay subprocess. The subprocess for Eq. (5) is shown in Fig. 3(c), without the decay of the Z and the matrix element squared is given in Appendix F. For $Z\to\nu\bar{\nu}$ decay, we multiply the matrix element squared of Appendix F by the $Z\to\nu\bar{\nu}$ branching fraction, $B(Z\to\nu\bar{\nu})=0.23$, assuming four generations of light neutrinos. The charge conjugates of the final states in Eqs. (2)–(5) are included in the calculations.

The most serious background to Eq. (2) arises from W-boson production and leptonic decay $pp\to W\to e\nu_e$. This background is more than an order of magnitude greater than the heavy-lepton signal in all kinematic ranges, as is evident from Fig. 4(a), which shows the $p_T(e)$ distribution for the signal and backgrounds. [Note that the $\not{p}_T$ and $p_T(e)$ distributions are the same in this case.] Contributions to the $W\to e\nu_e$ background with the W off-shell are highly significant; they produce the high-$p_T(e)$ tail. If this background is calculated with the W on the mass shell, the $p_T(e)$ distribution cuts off at $p_T(e)=\frac{1}{2}M_W$.

Also shown in Fig. 4(a) are the background contributions of Eqs. (4) and (5). The τ background contribution might be reduced somewhat by use of vertex detectors. No acceptance cuts have been imposed on the cross sections shown in this figure.

The overall background is more than an order of magnitude greater than the heavy-lepton signal for other measurable kinematic variables as well. Results for distributions in transverse mass, defined by

$$M_T^2(e,\not{p}_T)=(\,|\mathbf{p}_{eT}|+|\not{\mathbf{p}}_T|\,)^2-|\mathbf{p}_{eT}+\not{\mathbf{p}}_T|^2\ , \tag{6}$$

where the missing transverse momentum $\not{\mathbf{p}}_T$ is the sum of the transverse momenta carried away by the neutrinos, are qualitatively similar to the missing transverse momentum distributions. The rapidity distributions of the electron are shown in Fig. 4(b). The rapidity distributions of the W boson are similar to the electron rapidity distributions with the exception that the latter distributions fall off more steeply at large values of $|y|$. In all the distributions examined the signal and the backgrounds are similar in shape so acceptance cuts would not appreciably improve the signal-to-background ratio.

B. Hadronic decay of *L*

We next consider the hadronic decay mode $L\to\nu_L q\bar{q}'$. The subprocess is

$$d\bar{u}\to W^-\to L\bar{\nu}_L\ . \qquad \hookrightarrow \nu_L q\bar{q}' \tag{7}$$

The final state consists of $\not{p}_T$ and jets, the jets being formed from the final-state quarks. The heavy-lepton signal is compared to the following five standard-model backgrounds:

$$pp\to W^-\to\tau\bar{\nu}_\tau\ , \qquad \hookrightarrow \nu_\tau q\bar{q}' \tag{8}$$

$$pp\to Z^*,\gamma^*\to\tau\bar{\tau}\ , \qquad \hookrightarrow \bar{\nu}_\tau q_1\bar{q}_2, \quad \hookrightarrow \nu_\tau q_3\bar{q}_4 \tag{9}$$

$$pp\to ZZ\ , \qquad \hookrightarrow \nu\bar{\nu}, \quad \hookrightarrow q\bar{q} \tag{10}$$

$$pp \rightarrow WZ\ , \quad W \rightarrow q\bar{q}\,' ,\ Z \rightarrow \nu\bar{\nu} \tag{11}$$

$$pp \rightarrow Z + \text{jets}\ . \quad Z \rightarrow \nu\bar{\nu} \tag{12}$$

The charge conjugates of the final states in Eqs. (7), (8), and (11) are included in the calculations. The matrix elements squared for the subprocesses are given in Appendixes B, C, E, and F.

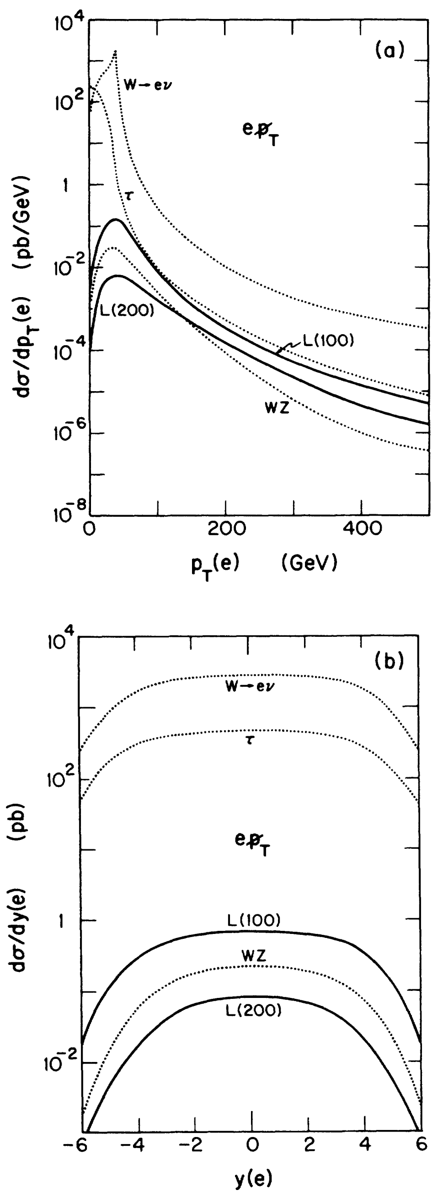

FIG. 4. Distributions for single-L production with leptonic decay: (a) transverse momentum of the electron (the missing-transverse-momentum distribution is identical) and (b) rapidity of the electron. Heavy-lepton signals for masses 100 and 200 GeV are denoted by solid curves. Backgrounds from $W \rightarrow e\nu_e$, $W \rightarrow \tau\nu_\tau$, and WZ are indicated by dotted curves; see Eqs. (3)–(5).

The $\not{p}_T$ distributions for both the signal and backgrounds are shown in Fig. 5(a) without cuts. The heavy-lepton signal is well below the $Z(\rightarrow\nu\bar{\nu})+\text{jets}$ background. One can improve the L signal-to-background ratio by using a cut on the invariant mass of the hadrons. Since the heavy leptons considered here are massive enough that they decay into a real $W, L \rightarrow \nu_L W$ with $W \rightarrow q\bar{q}\,'$, the two jets formed from q and $\bar{q}\,'$ will have a combined invariant-mass equal to M_W, i.e., $(p_{\text{jet }1}+p_{\text{jet }2})^2 = M_W^2$, where $p_{\text{jet }i}$ is the four-momentum of jet i. To exploit this constraint a cut was imposed on both the signal and background; only those events which contained two jets whose combined invariant mass M_{JJ} was within ± 5 GeV of M_W were accepted. Using the jet criteria described in Sec. II and $m_L = 100$ GeV, approximately 70% of the $L \rightarrow \nu_L q\bar{q}\,'$ events were found to contain two jets; thus not much of the signal is lost by imposing this cut. The $\not{p}_T$ distribution with this invariant-mass cut is shown in Fig. 5(b). This cut eliminates the ZZ and τ backgrounds and suppresses the other backgrounds, but the $Z(\rightarrow\nu\bar{\nu})+2$ jets background (the jet pair fakes the true two-jet W-decay) still exceeds the heavy-lepton signal.

We repeated the $Z+2$ jets background calculation with ISAJET (Ref. 9) version number 5.33, in which parton fragmentation to hadrons is taken into account and found results qualitatively similar to our parton-level shower calculations shown in Figs. 5(a) and 5(b). Similar results were also found when the $Z+2$ jets background calculation was repeated with PYTHIA (Ref. 10) version number 4.8. The assumption that the invariant mass of the jets can be measured to ± 5 GeV is perhaps optimistic; an uncertainty of ± 10 GeV makes the signal-to-background ratio worse by a factor of 2. Even with a two-jet invariant-mass cut of ± 2 GeV the $Z+2$ jets background is still slightly larger than the signal.

Perturbative calculations[15,16] of $Z+2$ jets to order α_s^2 can be used for a separate estimate of the backgrounds. The QCD Monte Carlo results presented here are within a factor of 2 of perturbative calculations.[17]

The rapidity distributions of the two-jet system for events with $M_{JJ} = M_W \pm 5$ GeV are shown in Fig. 5(c). Other kinematic distributions, such as the transverse momentum of the jets, the transverse opening angle between two jets, the jet polar angle, and x_{out}, are also plagued by an overwhelming background. Here the variable x_{out} considered previously for gluino detection[18] is defined by

$$x_{\text{out}} = \frac{\not{p}_T \cdot \hat{\mathbf{e}}_2}{\sum E_T(\text{hadrons})} \tag{13}$$

and

$$\hat{\mathbf{e}}_2 = \hat{\mathbf{z}} \times \hat{\mathbf{e}}_1\ , \tag{14}$$

where $\hat{\mathbf{e}}_1$ is the transverse direction of the jet with the largest E_T and $\hat{\mathbf{z}}$ is the beam direction

The p_T distributions of the individual jets are somewhat different for the heavy-lepton signal and the $(Z\rightarrow\nu\bar{\nu})+2$ jets background, as shown in Figs. 5(d) and

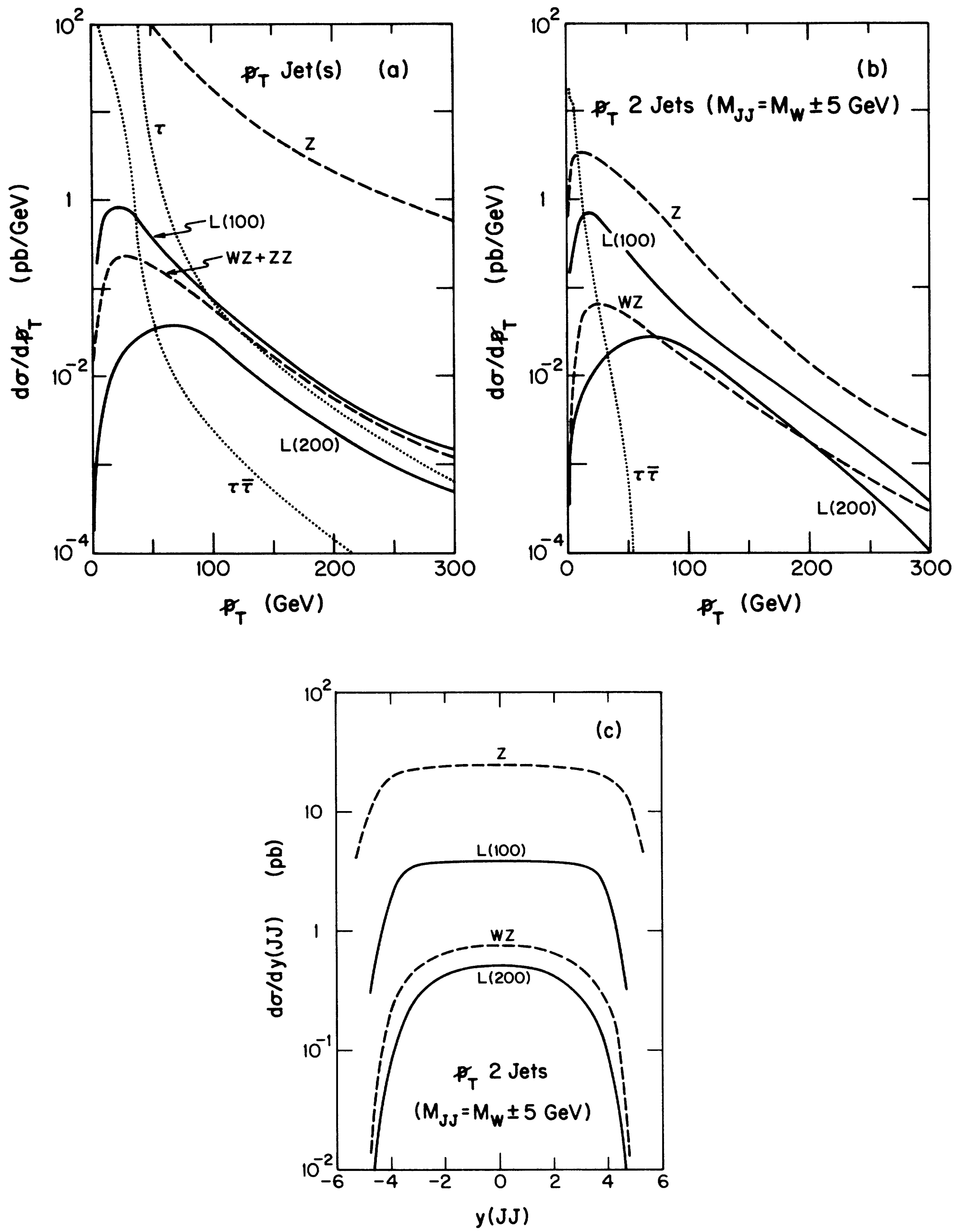

FIG. 5. Distributions for single-L production with hadronic decay: (a) missing transverse momentum without cuts, (b) missing transverse momentum for two-jet events with $M_{JJ}=M_W\pm5$ GeV, (c) rapidity of the two-jet system for events with $M_{JJ}=M_W\pm5$ GeV, (d) p_T of the fast jet (the jet with the largest p_T) for two-jet events with $M_{JJ}=M_W\pm5$ GeV, and (e) p_T of the slow jet for two-jet events with $M_{JJ}=M_W\pm5$ GeV. Heavy-lepton signals for masses of 100 and 200 GeV are shown with solid lines. Backgrounds from τ and $\tau\bar{\tau}$ are indicated by dotted curves, backgrounds from WZ, ZZ, and $pp\to Z+$jets are indicated by dashed curves; see Eqs. (7)–(12).

5(e). However, we were unable to appreciably improve the signal-to-background ratio by adjusting the cuts on the p_T and rapidity of the jets.

Even though the background is much larger than the signal, it may still be possible to observe the L signal in high-statistics measurements if the background is very well known.[17] However, it is unlikely that the QCD background can be predicted to better than 5% accuracy due to uncalculated higher-order corrections and a possible statistical observation of the L signal would suffer from a background uncertainty of this order. A more promising method to determine the background is to measure $(Z\to l\bar{l})+2$ jets events and multiply by the ratio of branching fractions $B(Z\to\nu\bar{\nu})/B(Z\to l\bar{l})$. With the background thus measured it may be possible to establish an L signal in $\not p_T+2$ jets events with high statistics.

C. $L\bar{L}$ pair production with leptonic decays

The production rates for $L\bar{L}$ pair production are much smaller than for single L, as shown in Fig. 2. On the oth-

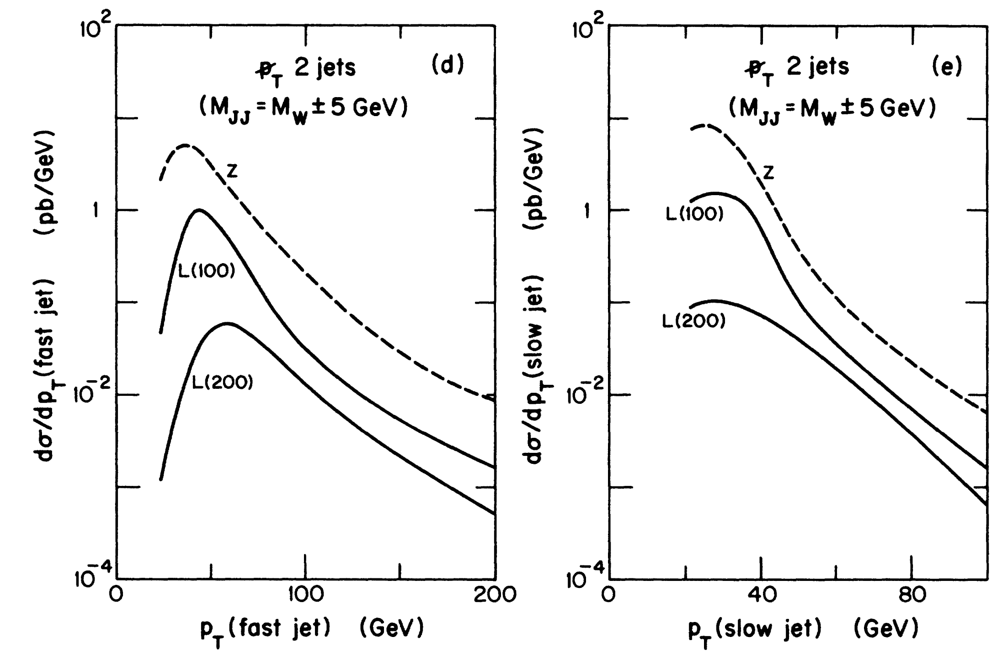

FIG. 5. (*Continued*).

er hand, the background rates are also smaller.

The $L\bar{L}$ pair is assumed to be produced via the Drell-Yan process $pp \to Z^*, \gamma^* \to L\bar{L}$ with both L and $\bar{L}$ decaying into leptons. The subprocess is

$$q\bar{q} \to Z^*, \gamma^* \to L\bar{L} \qquad (15)$$

$$\bar{L} \to \bar{\nu}_L \bar{e} \nu_e$$

$$L \to \nu_L e \bar{\nu}_e$$

corresponding to the Feynman diagram shown in Fig. 1(b); the matrix element squared is given in Appendix C. The signal for $L\bar{L}$ pair production with leptonic decays is an electron, a positron, and $\not p_T$ (or $\mu^-, \mu^+, \not p_T$ or $e^{\mp}, \mu^{\pm}, \not p_T$). This signal is compared to three standard-model backgrounds:

$$pp \to Z^*, \gamma^* \to \tau\bar{\tau} \, , \qquad (16)$$

$$\bar{\tau} \to \bar{\nu}_\tau \bar{e} \nu_e$$

$$\tau \to \nu_\tau e \bar{\nu}_e$$

$$pp \to W^+ W^- \, , \qquad (17)$$

$$W^- \to e\bar{\nu}_e$$

$$W^+ \to \bar{e}\nu_e$$

$$pp \to ZZ \, . \qquad (18)$$

$$Z \to \nu\bar{\nu}$$

$$Z \to e\bar{e}$$

The matrix elements squared for the subprocesses are given in Appendixes C–E. The ZZ background can be eliminated by rejecting events in which the invariant mass of the e^+e^- pair reconstruct the Z-boson mass; also this background does not contribute to $e\mu$ events.

Figure 6 shows distributions of $\not p_T$, the transverse momentum of the electron, the invariant mass of the e^+e^- pair, and the cluster transverse mass $M_T(e\bar{e}, \not p_T)$, which is defined by

$$M_T^2(e\bar{e}, \not p_T) = [(\, | \mathbf{p}_{e\bar{e}T} |^2 + m_{e\bar{e}}^2)^{1/2} + | \not \mathbf{p}_T | \,]^2 - | \mathbf{p}_{e\bar{e}T} + \not \mathbf{p}_T |^2 \, ,$$

where $\mathbf{p}_{e\bar{e}} = \mathbf{p}_e + \mathbf{p}_{\bar{e}}$ and $m_{e\bar{e}}^2 = (p_e + p_{\bar{e}})^2$. Also shown in Fig. 6 are the electron rapidity distributions. No cuts have been applied in these figures. The rapidity distributions of the W^- boson are again similar to the electron rapidity distributions with the exception that the latter distributions fall off more steeply at large values of $|y|$.

The $\tau\bar{\tau}$ background can be reduced by the cuts $p_T(e^{\pm}) > 20$ GeV, $\not p_T > 20$ GeV, $|y(e^{\pm})| < 5$, and $\Delta\phi(e^+e^-) < 160°$, where $\Delta\phi(e^+e^-)$ is the transverse opening angle between the e^+ and e^-. The $\tau\bar{\tau}$ background is rejected because the fast e^+ and e^- from the decaying $\tau\bar{\tau}$ pair must emerge nearly back-to-back in the transverse plane. Unfortunately, the W^+W^- background still overwhelms the $L\bar{L}$ signal as illustrated in Fig. 6(f), which shows the $p_T(e^-)$ distribution with the previously stated cuts imposed. A more restrictive cut on $\Delta\phi(e^+e^-)$, of say $\Delta\phi(e^+e^-) < 120°$, will completely eliminate the $\tau\bar{\tau}$ background, but will also reduce the $L\bar{L}$ signal. All curves in Fig. 6(f) include initial-state radiation effects, which were simulated by the QCD shower model of Ref. 8. Only events with no jets were selected for Fig. 6(f); with the jet criteria of Sec. II, approximately 40% of the $L\bar{L}$ and W^+W^- events contain no jets. Initial-state radiation has the most effect on the $\tau\bar{\tau}$ distributions; it allows the e^+ and e^- from the decaying $\tau\bar{\tau}$ pair to emerge at angles smaller than 180° in the trans-

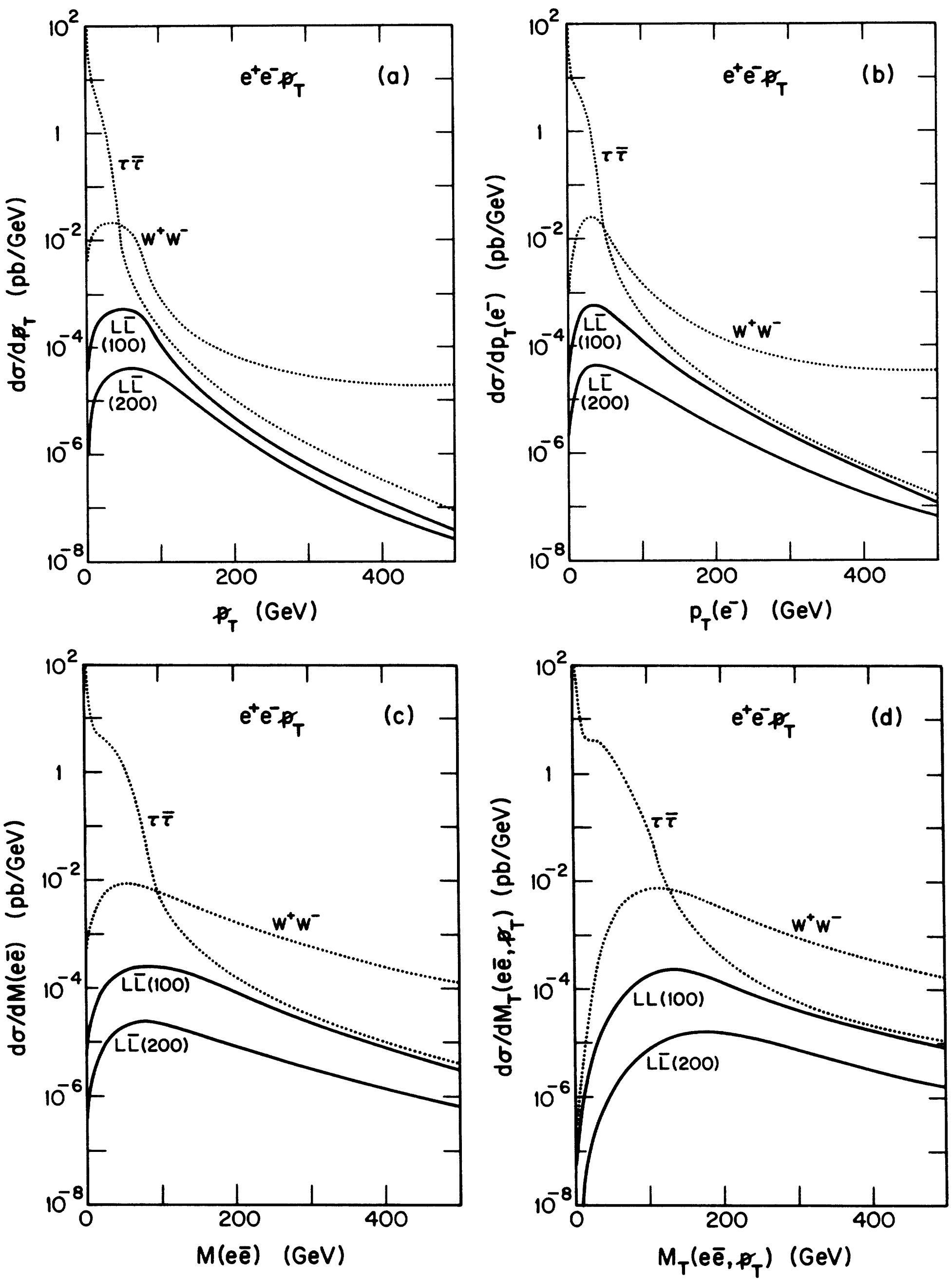

FIG. 6. Distributions for $L\bar{L}$ pair production with leptonic decays: (a) missing transverse momentum, (b) electron transverse momentum, (c) invariant mass of e^+e^- pair, (d) transverse cluster mass of e^+e^- pair and missing momentum, (e) electron rapidity, and (f) electron transverse momentum calculated with initial-state radiation and cuts described in the text. No cuts have been applied to (a)–(e). Heavy-lepton signals for masses of 100 and 200 GeV are shown with solid curves. Backgrounds from $\tau\bar{\tau}$ and W^+W^- are indicated by dotted curves; see Eqs. (15)–(18).

verse plane. The W^+W^- and $L\bar{L}$ distributions are less affected by initial-state radiation due to the heavier masses of the W and L particles.

D. $L\bar{L}$ pair production with one leptonic decay and one hadronic decay

Next we consider $L\bar{L}$ pair production, with one heavy lepton decaying into leptons while the other decays into hadrons. The subprocess is

$$q\bar{q} \to Z^*, \gamma^* \to L\bar{L} \; . \tag{19}$$
$$\bar{L} \to \bar{\nu}_L W^+ \to \bar{\nu}_L q\bar{q}\,'$$
$$L \to \nu_L W^- \to \nu_L e\bar{\nu}_e$$

The final state consists of an electron, $\not{p}_T$, and jets. With the jet criteria described in Sec. II and $m_L = 100$ GeV, the hadronic decay products will form two jets in 67% of these events.

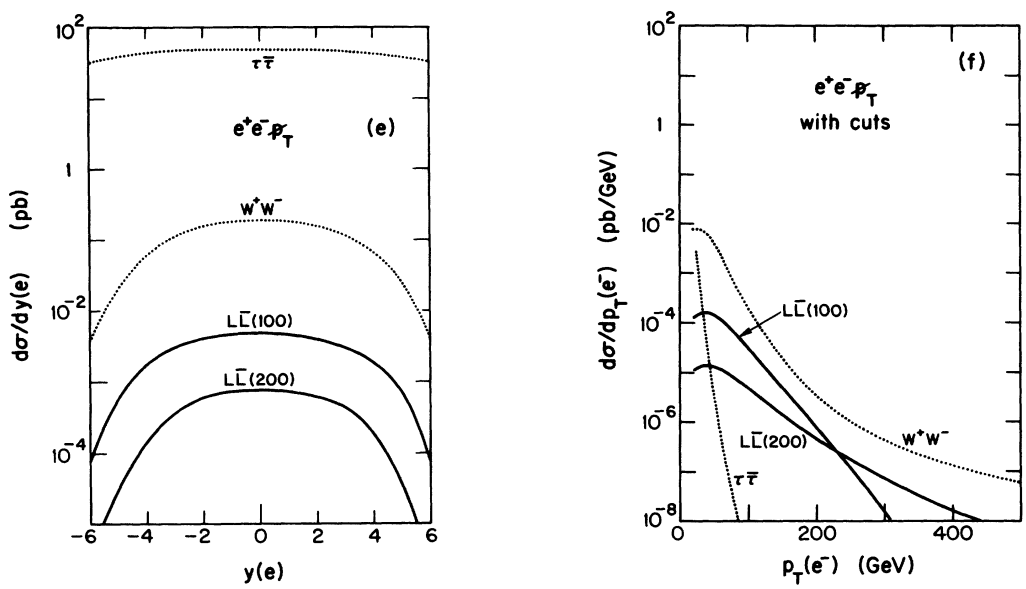

FIG. 6. (*Continued*).

Background processes for this decay scenario are

$$pp \to W^- + \text{jets}\ , \quad W^- \to e\bar{\nu}_e \tag{20}$$

$$pp \to W^+W^-\ . \quad W^- \to e\bar{\nu}_e,\ W^+ \to q\bar{q}'\ . \tag{21}$$

The matrix element squared for the subprocess in Eq. (21) is given in Appendix D. To suppress the background, only events containing two jets whose combined invariant mass is equal to $M_W \pm 5$ GeV are chosen. This cut suppresses the background from $pp \to W^- +$jets below that from the W^+W^- continuum at large $p_T(e)$. [In Ref. 15 the $W+2$ jets contribution dominated the W^+W^- contribution; however, the $p_T(e)$ distribution was not considered.] Figure 7 shows distributions for $\not p_T$, $p_T(e)$, and $M_T(e,\not p_T)$. In all cases, the heavy-lepton signal is below the background. This is also true for other distributions such as x_{out}, the electron polar angle, the transverse opening angle between two jets, and the transverse opening angle between the electron and the missing momentum.

In the case of $e^+e^- \to W^+W^-$ the W^- is produced

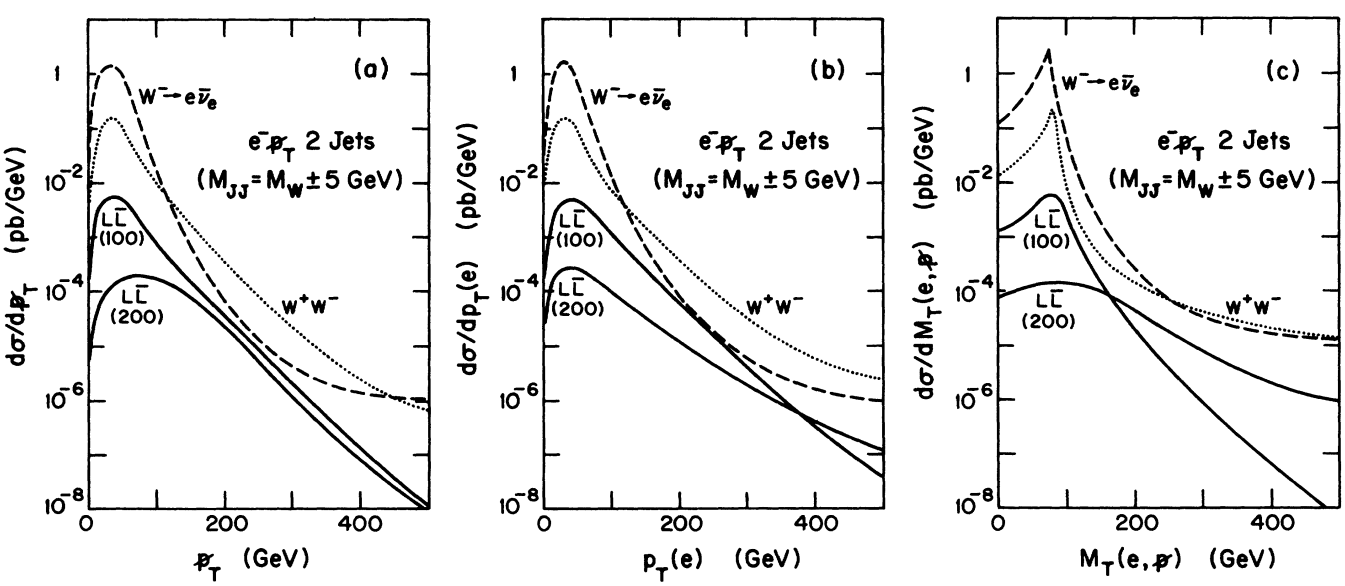

FIG. 7. Distributions for $L\bar{L}$ pair production with one leptonic and one hadronic decay for two-jet events with $M_{JJ} = M_W \pm 5$ GeV: (a) missing transverse momentum, (b) electron transverse momentum, and (c) transverse mass of the electron and missing momentum. Heavy-lepton signals for masses of 100 and 200 GeV are shown with solid curves. The background from W^+W^- is indicated by the dotted curve and the background from $pp \to W^- + 2$ jets is indicated by dashed curves; see Eqs. (19)–(21).

preferentially in the direction of the incident electron;[19] thus the W^+W^- background can be suppressed by rejecting events which have a small angle θ^* between the e^- and W^- in the W^+W^- rest frame. In $pp \to W^+W^-$, with θ^* the angle in the W^+W^- rest frame between the W^+ and the proton beam direction, the distribution is symmetric about $\cos\theta^* = 0$ and peaked in the beam directions ($\cos\theta^* = \pm 1$), falling by an order of magnitude to a minimum at $\cos\theta^* = 0$. In contrast, the $\cos\theta^*$ distribution of the W^+ from the decay of $L\bar{L}$ is relatively flat, but it is also an order of magnitude below the $pp \to W^+W^-$ background even at $\cos\theta^* = 0$. Even if the invariant-mass distribution of the W^+W^- pair could be measured, it would not be useful for separating the $L\bar{L}$ signal from the $pp \to W^+W^-$ background because the distributions are qualitatively similar and the $L\bar{L}$ is at least an order of magnitude below the background.

E. $L\bar{L}$ pair production with hadronic decays

The final heavy lepton signal to be considered is $L\bar{L}$ pair production, with both heavy leptons decaying into hadrons. The subprocess is

$$q\bar{q} \to Z^*, \gamma^* \to L\bar{L} \; . \qquad (22)$$
$$\bar{L} \to \bar{\nu}_L W^+ \to \bar{\nu}_L q_1 \bar{q}_2$$
$$L \to \nu_L W^- \to \nu_L q_3 \bar{q}_4$$

The hadronic decay of an $L\bar{L}$ pair provides a distinctive signature; the heavy leptons decay into real W bosons and each W boson can in turn decay into two jets whose combined invariant mass is M_W. With the jet criteria described in Sec. II and $m_L = 100$ GeV, this happens in 42% of the $L\bar{L}$ events which decay into hadrons. A criterion for selecting such an event is that it contain four jets, with two pairs of the jets having a combined invariant mass equal to $M_W \pm 5$ GeV. The value ± 5 GeV was chosen as an optimistic experimental uncertainty. The only background source is $pp \to Z + 4$ jets, with $Z \to \nu\bar{\nu}$.

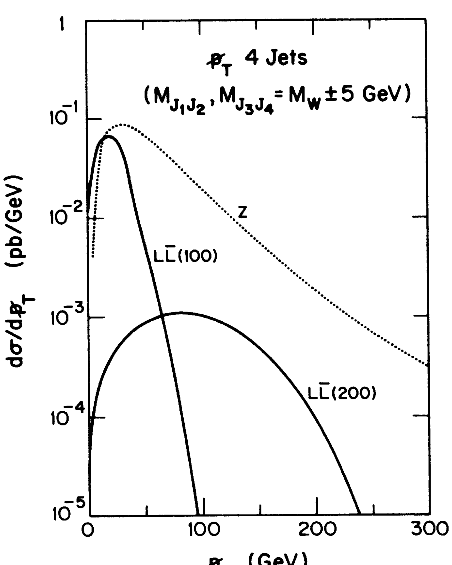

FIG. 8. Missing transverse momentum for $L\bar{L}$ pair production with hadronic decays for four-jet events with $M_{J_1J_2} = M_W \pm 5$ GeV and $M_{J_3J_4} = M_W \pm 5$ GeV. Heavy-lepton signals for masses of 100 and 200 GeV are shown with solid curves. Background from $pp \to Z + 4$ jets is indicated by the dotted curve; see Eqs. (22) and (12).

Figure 8 shows the $\not{p}_T$ distribution for the signal and background, with the above cuts imposed. Except for the region $\not{p}_T \lesssim 15$ GeV, which would be below the observable $\not{p}_T$ threshold, the background is still above the signal even with these stringent cuts. One might think that microvertex detectors could help distinguish the charm jet in $L \to \nu_L c\bar{s}$ decays from the gluon and light-quark jets in the $pp \to Z +$jets background; however, the charm multiplicity from gluon jets[20] grows rapidly with p_T and thus the presence of charm is not a useful indicator of L production and decay. Again the background here can be inferred from measurements of $(Z \to l\bar{l}) + 4$ jets events and the L signal thereby established from high-statistics measurements of $\not{p}_T + 4$ jets events.

IV. CONCLUSIONS

The results presented here indicate that it will not be easy to detect a heavy lepton, with mass $m_L > M_W$ and $m_{\nu_L} \approx 0$, at the SSC or at the LHC. The dominant background sources are weak bosons produced either singly or in pairs. These backgrounds are at least an order of magnitude greater than the heavy-lepton signals. This is true for all kinematic ranges of all distributions examined. The signal and background are often qualitatively similar, which seems to preclude the use of selective cuts to directly separate the signal from the background. It may still be possible to detect a heavy lepton from its contribution to $\not{p}_T + 2$ or 4 jets events, where the $(Z \to \nu\bar{\nu}) + 2$ or 4 jets background may be determined from measurements of $(Z \to l\bar{l}) + 2$ or 4 jets events.

ACKNOWLEDGMENTS

We thank D. Froidevaux for private communication regarding a similar analysis. We thank H. Baer, J. Cudell, N. Glover, T. Gottschalk, G. Kane, F. Paige, S. Ritz, R. Stroynowiski, X. Tata, and S. Willenbrock for discussions. This research was supported in part by the University of Wisconsin Research Committee with funds granted by the Wisconsin Alumni Research Foundation and in part by the U.S. Department of Energy under Contract No. DE-AC02-76ER00881.

APPENDIX A: NOTATION AND CONVENTIONS

The matrix elements squared, summed (averaged) over final (initial) spins and colors, for the subprocesses considered in this paper are presented in the following appendixes. The notation and conventions common to these appendixes are defined here.

Particle labels are used to denote their four-momentum, $U_{qq'}$ denotes a Kobayashi-Maskawa (KM) quark-mixing-matrix element, and $|D_X(X)|^2$ denotes the squared propagator for particle X:

$$|D_X(X)|^2=[(X^2-M_X^2)^2+(\Gamma_X M_X)^2]^{-1} . \tag{A1}$$

The vector and axial-vector couplings of the Z boson to fermions are denoted by

$$g_V^i=T_3^i-2x_W Q^i,\quad g_A^i=T_3^i , \tag{A2}$$

where T_3^i and Q^i are the third component of weak isospin and the electric charge of the associated quark or lepton i. Also $x_W=\sin^2\theta_W$, where θ_W is the Weinberg angle.

Standard conventions are used so that a cross-section formula for a subprocess with n particles in the final state is

$$d\sigma(q_1+q_2\to p_1+\cdots+p_n)=\frac{1}{2\hat{s}}|\mathcal{M}|^2\prod_{i=1}^{n}\left[\frac{d^3\mathbf{p}_i}{(2\pi)^3 2E_i}\right](2\pi)^4\delta^4\left[q_1+q_2-\sum_{i=1}^{n}p_i\right] . \tag{A3}$$

The results given in these appendixes are for leptonic decays of the weak bosons; for hadronic decay include a color factor of 3 for each decaying weak boson and a quark-mixing-matrix element squared $|U_{qq'}|^2$ for each decaying W boson.

APPENDIX B: MATRIX ELEMENT SQUARED FOR L PRODUCTION AND DECAY

The L is produced via $d\bar{u}\to W\to L\bar{\nu}_L$ and decays via $L\to\nu_L e\bar{\nu}_e$. The Feynman diagram for this process is shown in Fig. 1(a). The squared matrix element for this process is straightforward to calculate and has been given in the literature.[1] It is reproduced here for completeness. The squared matrix element, averaged over initial spins and colors, is

$$|\mathcal{M}|^2=\tfrac{1}{4}\langle\tfrac{1}{3}\rangle 16\left[\frac{4\pi\alpha}{x_W}\right]^4|U_{ud}|^2|D_W(W_1)|^2|D_W(W_2)|^2|D_L(L)|^2(d\cdot\bar{\nu}_L)(e\cdot\nu_L)[(\bar{u}\cdot L)(\bar{\nu}_e\cdot L)-\tfrac{1}{2}m_L^2(\bar{u}\cdot\bar{\nu}_e)] . \tag{B1}$$

APPENDIX C: MATRIX ELEMENT SQUARED FOR $L\bar{L}$ PRODUCTION AND DECAY

The $L\bar{L}$ are produced via the Drell-Yan process $q\bar{q}\to\gamma^*,Z^*\to L\bar{L}$ and decay via $L\to\nu_L e\bar{\nu}_e$ and $\bar{L}\to\bar{\nu}_L\bar{e}\nu_e$. The Feynman diagram for this process is shown in Fig. 1(b). Contributions from virtual Z^* exchange, virtual-photon exchange, and their interference are included. The matrix element squared was calculated using the helicity-projection techniques described in Ref. 21. The results for the Z^*-exchange and virtual-photon-exchange terms agree with the results given in Ref. 22 (the interference term was neglected in this reference).

The complete matrix element squared, averaged over initial spins and colors, has the form

$$|\mathcal{M}|^2=\tfrac{1}{4}\langle\tfrac{1}{3}\rangle A[|\mathcal{M}_Z|^2+|\mathcal{M}_\gamma|^2+2\,\mathrm{Re}(\mathcal{M}_Z\mathcal{M}_\gamma^\dagger)] , \tag{C1}$$

where the three terms correspond to Z^* exchange, γ^* exchange, and Z^*-γ^* interference. The factor $\frac{1}{4}$ is from averaging over initial spins, the $\langle\frac{1}{3}\rangle$ is a color factor, and the common factor A is

$$A=16\left[\frac{4\pi\alpha}{x_W}\right]^4(e\cdot\nu_L)(\bar{e}\cdot\bar{\nu}_L)|D_W(W^-)|^2|D_W(W^+)|^2|D_L(L)|^2|D_L(\bar{L})|^2 . \tag{C2}$$

The three terms in the equation for $|\mathcal{M}|^2$ can be written

$$|\mathcal{M}_Z|^2=B_Z\sum_{i=1}^{6}C_i^Z X_i,\quad |\mathcal{M}_\gamma|^2=B_\gamma\sum_{i=1}^{6}C_i^\gamma X_i,\quad 2\,\mathrm{Re}(\mathcal{M}_Z\mathcal{M}_\gamma^\dagger)=B_I\sum_{i=1}^{6}C_i^I X_i , \tag{C3}$$

where the X_i factors are

$$\begin{aligned}
&X_1=m_L^4(q\cdot\bar{\nu}_e)(\nu_e\cdot\bar{q}),\quad X_2=m_L^4(q\cdot\nu_e)(\bar{q}\cdot\bar{\nu}_e) ,\\
&X_3=(\bar{q}\cdot\bar{L})(\nu_e\cdot\bar{L})[(q\cdot L)(\bar{\nu}_e\cdot L)-m_L^2(q\cdot\bar{\nu}_e)]+(q\cdot L)(\bar{\nu}_e\cdot L)[(\bar{q}\cdot\bar{L})(\nu_e\cdot\bar{L})-m_L^2(\bar{q}\cdot\nu_e)] ,\\
&X_4=X_3(q\leftrightarrow\bar{q}) ,\\
&X_5=m_L^2\{(q\cdot\bar{q})[(L\cdot\nu_e)(\bar{L}\cdot\bar{\nu}_e)+(L\cdot\bar{\nu}_e)(\bar{L}\cdot\nu_e)-(L\cdot\bar{L})(\nu_e\cdot\bar{\nu}_e)]+(\nu_e\cdot\bar{\nu}_e)[(L\cdot q)(\bar{L}\cdot\bar{q})+(L\cdot\bar{q})(\bar{L}\cdot q)]\\
&\qquad+(L\cdot\bar{L})[(q\cdot\bar{\nu}_e)(\bar{q}\cdot\nu_e)+(q\cdot\nu_e)(\bar{q}\cdot\bar{\nu}_e)]-(\bar{L}\cdot\bar{\nu}_e)[(q\cdot\nu_e)(L\cdot\bar{q})+(\bar{q}\cdot\nu_e)(L\cdot q)]\\
&\qquad-(L\cdot\nu_e)[(q\cdot\bar{\nu}_e)(\bar{L}\cdot\bar{q})+(\bar{q}\cdot\bar{\nu}_e)(q\cdot\bar{L})]\} ,\\
&X_6=m_L^2\{(\nu_e\cdot\bar{L})[(\bar{q}\cdot L)(q\cdot\bar{\nu}_e)-(q\cdot L)(\bar{q}\cdot\bar{\nu}_e)]+(\bar{\nu}_e\cdot L)[(q\cdot\bar{L})(\bar{q}\cdot\nu_e)-(\bar{q}\cdot\bar{L})(q\cdot\nu_e)]\} .
\end{aligned} \tag{C4}$$

The B factors are

$$B_Z=\left[\frac{4\pi\alpha}{x_W(1-x_W)}\right]^2 |D_Z(Z)|^2 ,$$
$$B_\gamma=8\left[\frac{4\pi\alpha Q_q}{\hat{s}}\right]^2 , \tag{C5}$$
$$B_I=-4Q_q\frac{(4\pi\alpha)^2}{x_W(1-x_W)}(1-M_Z^2/\hat{s})|D_Z(Z)|^2 ,$$

where Q_q is the fractional electric charge of the initial quark and $\hat{s}=(q+\bar{q})^2$. The C factors are combinations of the Z boson to fermion couplings. The C_i^Z factors are

$$C_{1,2}^Z=\tfrac{1}{2}[(g_V^q)^2+(g_A^q)^2][(g_V^L)^2+(g_A^L)^2]\mp 2g_V^q g_A^q g_V^L g_A^L ,$$
$$C_{3,4}^Z=\tfrac{1}{2}(g_V^q\mp g_A^q)^2(g_V^L+g_A^L)^2 , \tag{C6}$$
$$C_5^Z=\tfrac{1}{2}[(g_V^q)^2+(g_A^q)^2][(g_V^L)^2-(g_A^L)^2] ,$$
$$C_6^Z=g_V^q g_A^q[(g_V^L)^2-(g_A^L)^2] .$$

The C_i^γ factors are all unity, except for C_6^γ which vanishes. The C_i^I factors are

$$C_{1,2}^I=(g_V^q g_V^L\mp g_A^q g_A^L),\quad C_5^I=g_V^q g_V^L ,$$
$$C_{3,4}^I=(g_V^q\mp g_A^q)(g_V^L+g_A^L),\quad C_6^I=g_A^q g_V^L . \tag{C7}$$

With the conventions stated in Eq. (A2), the Z boson to fermion couplings are explicitly

$$g_V^L=-\tfrac{1}{2}+2x_W,\quad g_A^L=-\tfrac{1}{2} ,$$
$$g_V^u=\tfrac{1}{2}-\tfrac{4}{3}x_W,\quad g_A^u=\tfrac{1}{2} , \tag{C8}$$
$$g_V^d=-\tfrac{1}{2}+\tfrac{2}{3}x_W,\quad g_A^d=-\tfrac{1}{2} .$$

APPENDIX D: MATRIX ELEMENT SQUARED FOR W^+W^- PRODUCTION AND DECAY

The process considered is

$$q\bar{q}'\to W^+W^- \tag{D1}$$
$$W^-\to e\bar{\nu}_e$$
$$W^+\to \bar{e}\nu_e$$

corresponding to the Feynman diagrams in Fig. 3(a). The traces of gamma matrices were evaluated using the algebraic computer programs REDUCE and SCHOONSCHIP. The spin/color-averaged matrix element squared can be written

$$|\mathcal{M}|^2=\tfrac{1}{4}\langle\tfrac{1}{3}\rangle A(|\mathcal{M}_u|^2+|\mathcal{M}_d|^2+|\mathcal{M}_\gamma|^2+|\mathcal{M}_Z|^2+I_{u\gamma}+I_{d\gamma}+I_{uZ}+I_{dZ}+I_{Z\gamma}) . \tag{D2}$$

The $|\mathcal{M}_i|^2$ terms represent the square of a graph, while the I_{ij} terms represent the interference between two graphs. These terms can be written

$$|\mathcal{M}_u|^2=\frac{|U_{ud}|^4}{\hat{u}^2}T_1,\quad |\mathcal{M}_d|^2=\frac{|U_{ud}|^4}{\hat{t}^2}T_2 ,$$
$$|\mathcal{M}_\gamma|^2=\frac{4Q_q^2x_W^2}{\hat{s}^2}T_3 ,$$
$$|\mathcal{M}_Z|^2=\{[(g_V^q)^2+(g_A^q)^2]T_3-2g_V^q g_A^q T_4\}|D_Z(Z)|^2 , \tag{D3}$$

$$I_{u\gamma}=\frac{2Q_u x_W|U_{ud}|^2}{\hat{s}\hat{u}}T_5,\quad I_{d\gamma}=\frac{2Q_d x_W|U_{ud}|^2}{\hat{s}\hat{t}}T_6 ,$$
$$I_{uZ}=\frac{|U_{ud}|^2}{\hat{u}}|D_Z(Z)|^2(\hat{s}-M_Z^2)(g_V^u+g_A^u)T_5 ,$$
$$I_{dZ}=\frac{|U_{ud}|^2}{\hat{t}}|D_Z(Z)|^2(\hat{s}-M_Z^2)(g_V^d+g_A^d)T_6 ,$$
$$I_{Z\gamma}=\frac{4Q_q x_W}{\hat{s}}|D_Z(Z)|^2(\hat{s}-M_Z^2)(g_V^q T_3-g_A^q T_4) .$$

The T factors are, up to powers of 2, the results of traces of gamma matrices. The common factor A is

$$A=16\left[\frac{4\pi\alpha}{x_W}\right]^4|D_W(W^-)|^2|D_W(W^+)|^2 , \tag{D4}$$

Q_i is the fractional electric charge of quark i and the Mandelstam variables are

$$\hat{s}=(q+\bar{q}')^2,\quad \hat{t}=(q-W^-)^2,\quad \hat{u}=(q-W^+)^2 . \tag{D5}$$

The T factors are listed next, where for convenience ν_e and $\bar{q}'$ are written as ν and $\bar{q}$.

$$T_1=(e\cdot\bar{q})(q\cdot\bar{e})[(q\cdot\nu)(q\cdot\bar{\nu})-(q\cdot\nu)(\bar{e}\cdot\bar{\nu})+(q\cdot\bar{e})(\nu\cdot\bar{\nu})-(q\cdot\bar{\nu})(\nu\cdot\bar{e})+(\nu\cdot\bar{e})(\bar{e}\cdot\bar{\nu})] ,$$

$$T_2=T_1(e\leftrightarrow\nu,\ \bar{e}\leftrightarrow\bar{\nu}) ,$$

$$T_3=2[-(e\cdot q)(e\cdot\bar{q})(\nu\cdot\bar{\nu})(\bar{e}\cdot\bar{\nu})-(e\cdot\nu)(e\cdot\bar{e})(q\cdot\bar{\nu})(\bar{q}\cdot\bar{\nu})-(e\cdot\nu)(e\cdot\bar{\nu})(q\cdot\bar{q})(\bar{e}\cdot\bar{\nu})$$
$$+(e\cdot\nu)(e\cdot\bar{\nu})(q\cdot\bar{e})(\bar{q}\cdot\bar{e})+(e\cdot\bar{\nu})(q\cdot\nu)(\nu\cdot\bar{q})(\bar{e}\cdot\bar{\nu})]+\tilde{T}_3+\tilde{T}_3(e\leftrightarrow\bar{\nu},\ \bar{e}\leftrightarrow\nu) ,$$

$$\begin{aligned}
\tilde{T}_3 = &(e\cdot q)(e\cdot v)(e\cdot\bar{v})(\bar{q}\cdot\bar{e})+(e\cdot q)(e\cdot v)(v\cdot\bar{v})(\bar{q}\cdot\bar{e})+(e\cdot q)(e\cdot\bar{e})(v\cdot\bar{v})(\bar{q}\cdot\bar{e})\\
&+(e\cdot q)(e\cdot\bar{e})(v\cdot\bar{v})(\bar{q}\cdot\bar{v})+(e\cdot q)(e\cdot\bar{v})(v\cdot\bar{q})(\bar{e}\cdot\bar{v})-(e\cdot q)(e\cdot\bar{v})(v\cdot\bar{e})(\bar{q}\cdot\bar{e})\\
&-(e\cdot q)(e\cdot\bar{v})(v\cdot\bar{e})(\bar{q}\cdot\bar{v})+(e\cdot v)(e\cdot\bar{q})(q\cdot\bar{v})(\bar{e}\cdot\bar{v})-(e\cdot v)(e\cdot\bar{e})(q\cdot\bar{v})(\bar{q}\cdot\bar{e})\\
&+(e\cdot v)(e\cdot\bar{v})(q\cdot v)(\bar{q}\cdot\bar{e})+(e\cdot v)(e\cdot\bar{v})(q\cdot\bar{e})(\bar{q}\cdot\bar{v})+(e\cdot v)(q\cdot v)(v\cdot\bar{v})(\bar{q}\cdot\bar{e})\\
&+(e\cdot v)(q\cdot v)(\bar{e}\cdot\bar{q})(\bar{e}\cdot\bar{v})-(e\cdot\bar{q})(q\cdot v)(v\cdot\bar{v})(\bar{e}\cdot\bar{v})+(e\cdot\bar{e})(q\cdot v)(v\cdot\bar{v})(\bar{q}\cdot\bar{e})\\
&+(e\cdot\bar{e})(q\cdot v)(v\cdot\bar{v})(\bar{q}\cdot\bar{v})+(e\cdot\bar{e})(q\cdot v)(\bar{q}\cdot\bar{e})(\bar{e}\cdot\bar{v})+(e\cdot\bar{e})(q\cdot v)(\bar{q}\cdot\bar{v})(\bar{e}\cdot\bar{v})\\
&-(e\cdot\bar{v})(q\cdot v)(v\cdot\bar{e})(\bar{q}\cdot\bar{e})-(e\cdot\bar{v})(q\cdot v)(v\cdot\bar{e})(\bar{q}\cdot\bar{v})+(e\cdot\bar{v})(q\cdot v)(\bar{q}\cdot\bar{e})(\bar{e}\cdot\bar{v})\\
&+(e\cdot\bar{v})(q\cdot v)(\bar{q}\cdot\bar{v})(\bar{e}\cdot\bar{v})-(q\cdot\bar{v})(\bar{q}\cdot\bar{e})(e\cdot v)^2-(e\cdot\bar{q})(q\cdot v)(\bar{e}\cdot\bar{v})^2\ ,
\end{aligned}$$

$$T_4=\tilde{T}_3-\tilde{T}_3(e\leftrightarrow\bar{v},\bar{e}\leftrightarrow v)\ ,$$

$$\begin{aligned}
T_5 = &(e\cdot q)(e\cdot v)(\bar{q}\cdot\bar{v})(\bar{e}\cdot\bar{v})-(e\cdot q)(e\cdot\bar{q})(v\cdot\bar{v})(\bar{e}\cdot\bar{v})-(e\cdot q)(v\cdot\bar{q})(\bar{q}\cdot\bar{v})(\bar{e}\cdot\bar{v})\\
&+(e\cdot v)(e\cdot\bar{q})(q\cdot\bar{e})(v\cdot\bar{v})-(e\cdot v)(e\cdot\bar{q})(q\cdot\bar{e})(\bar{q}\cdot\bar{v})-(e\cdot v)(e\cdot\bar{e})(q\cdot\bar{e})(\bar{q}\cdot\bar{v})\\
&-(e\cdot v)(e\cdot\bar{e})(q\cdot\bar{v})(\bar{q}\cdot\bar{v})-(e\cdot v)(e\cdot\bar{v})(q\cdot\bar{q})(\bar{e}\cdot\bar{v})+(e\cdot v)(e\cdot\bar{v})(q\cdot\bar{e})(v\cdot\bar{q})\\
&+(e\cdot v)(e\cdot\bar{v})(q\cdot\bar{e})(\bar{e}\cdot\bar{q})+(e\cdot v)(e\cdot\bar{v})(q\cdot\bar{v})(\bar{q}\cdot\bar{e})+(e\cdot v)(q\cdot\bar{e})(v\cdot\bar{q})(\bar{q}\cdot\bar{v})\\
&+(e\cdot\bar{q})(e\cdot\bar{e})(q\cdot\bar{e})(v\cdot\bar{v})+(e\cdot\bar{q})(e\cdot\bar{e})(q\cdot\bar{v})(v\cdot\bar{v})+(e\cdot\bar{q})(e\cdot\bar{v})(q\cdot v)(\bar{e}\cdot\bar{v})\\
&-(e\cdot\bar{q})(e\cdot\bar{v})(q\cdot\bar{e})(v\cdot\bar{q})-(e\cdot\bar{q})(e\cdot\bar{v})(q\cdot\bar{e})(v\cdot\bar{e})-(e\cdot\bar{q})(e\cdot\bar{v})(q\cdot\bar{v})(v\cdot\bar{e})\\
&+(e\cdot\bar{q})(q\cdot\bar{e})(v\cdot\bar{q})(v\cdot\bar{v})+(e\cdot\bar{q})(q\cdot\bar{e})(v\cdot\bar{q})(\bar{e}\cdot\bar{v})+(e\cdot\bar{e})(q\cdot\bar{e})(v\cdot\bar{q})(\bar{q}\cdot\bar{v})\\
&+(e\cdot\bar{e})(q\cdot\bar{v})(v\cdot\bar{q})(\bar{q}\cdot\bar{v})+(e\cdot\bar{v})(q\cdot\bar{q})(v\cdot\bar{q})(\bar{e}\cdot\bar{v})-(e\cdot\bar{v})(q\cdot\bar{e})(v\cdot\bar{q})(\bar{q}\cdot\bar{e})\\
&-(e\cdot\bar{v})(q\cdot\bar{v})(v\cdot\bar{q})(\bar{q}\cdot\bar{e})-(q\cdot\bar{e})(\bar{q}\cdot\bar{v})(e\cdot v)^2+(q\cdot\bar{e})(v\cdot\bar{v})(e\cdot\bar{q})^2-(e\cdot\bar{v})(q\cdot\bar{e})(v\cdot\bar{q})^2+2(e\cdot v)(e\cdot\bar{q})(e\cdot\bar{v})(q\cdot\bar{e})\ ,
\end{aligned}$$

$$T_6=-T_5(q\leftrightarrow\bar{q},e\leftrightarrow\bar{v},\bar{e}\leftrightarrow v)\ .$$

These formulas numerically reproduce the cross section results of Ref. 23 for real W^+W^- production.

APPENDIX E: MATRIX ELEMENT SQUARED FOR ZZ PRODUCTION AND DECAY

The process considered is

$$q\bar{q}\to ZZ,\quad Z\to f\bar{f},\quad Z\to f'\bar{f}' \tag{E1}$$

corresponding to the Feynman diagrams in Fig. 3(b). The results given here are general; f and f' can be any two different massless fermions. (If f and f' are identical fermions, the final state must be antisymmetrized.) The traces of gamma matrices were evaluated using the algebraic computer programs REDUCE and SCHOONSCHIP. The spin/color-averaged matrix element squared can be written

$$|\mathcal{M}|^2=\tfrac{1}{4}\langle\tfrac{1}{3}\rangle\left[\frac{4\pi\alpha}{x_W(1-x_W)}\right]^4|D_Z(Z_1)|^2|D_Z(Z_2)|^2\left[\frac{X_{\hat t}}{\hat t_2}+\frac{X_{\hat u}}{\hat u_2}+\frac{2X_I}{\hat t\hat u}\right]\ . \tag{E2}$$

The three terms arise from the squares of the two graphs and their interference. The Mandelstam variables are

$$\hat t=(q-f-\bar f)^2,\quad \hat u=(f+\bar f-\bar q)^2\ . \tag{E3}$$

The X terms are

$$\begin{aligned}
X_{\hat t}= &A(q\cdot\bar f)(f'\cdot\bar q)[2(K\cdot f)(K\cdot\bar f')-\hat t(f\cdot\bar f')]+B(q\cdot f)(f'\cdot\bar q)[2(K\cdot\bar f)(K\cdot\bar f')-\hat t(\bar f\cdot\bar f')]\\
&+C(q\cdot\bar f)(\bar f'\cdot\bar q)[2(K\cdot f)(K\cdot f')-\hat t(f\cdot f')]+D(q\cdot f)(\bar f'\cdot\bar q)[2(K\cdot\bar f)(K\cdot f')-\hat t(\bar f\cdot f')]\ ,\\
X_{\hat u}= &X_{\hat t}(K\to J,\hat t\to\hat u,q\leftrightarrow\bar q,f\leftrightarrow\bar f,f'\leftrightarrow\bar f')\ ,\\
X_I= &A(T_1+\bar T_1)+B(T_2+\bar T_2)+C(T_3+\bar T_3)+D(T_4+\bar T_4)+4E(T_7+\bar T_7)+(A+B)T_5+(C+D)T_5(q\leftrightarrow\bar q)\\
&+(A+C)T_6+(B+D)T_6(q\leftrightarrow\bar q)+(A+D)(f\cdot\bar f)(q\cdot\bar q)(f\cdot f')(\bar f\cdot\bar f')+(B+C)(f\cdot\bar f)(q\cdot\bar q)(f\cdot\bar f')(\bar f\cdot f')\ ,
\end{aligned} \tag{E4}$$

where the T_i terms are

$$\begin{aligned}
T_1&=(f\cdot f')(f\cdot q)(q\cdot\bar f')(\bar q\cdot\bar f)-(f\cdot f')(f\cdot\bar f)(q\cdot\bar q)(q\cdot\bar f')-(f\cdot f')(f\cdot\bar f)(q\cdot\bar f)(\bar q\cdot\bar f')-(f\cdot q)(f\cdot\bar q)(f'\cdot\bar f)(q\cdot\bar f')\ ,\\
T_2&=(f\cdot\bar q)(f\cdot\bar f')(f'\cdot\bar q)(q\cdot\bar f)-(f\cdot\bar f)(f'\cdot\bar f)(q\cdot\bar q)(q\cdot\bar f')-(f\cdot f')(q\cdot\bar f)(q\cdot\bar f')(\bar q\cdot\bar f)-(f\cdot\bar f)(f\cdot\bar f')(f'\cdot q)(\bar q\cdot\bar f)\ ,\\
T_3&=(f\cdot q)(f\cdot\bar f')(f'\cdot q)(\bar q\cdot\bar f)-(f\cdot\bar q)(f\cdot\bar f)(f'\cdot\bar f)(q\cdot\bar f')-(f\cdot q)(f\cdot\bar q)(f'\cdot q)(\bar f\cdot\bar f')-(f\cdot\bar f)(f\cdot\bar f')(f'\cdot q)(q\cdot\bar q)\ ,\\
T_4&=(f\cdot f')(f\cdot\bar q)(q\cdot\bar f)(\bar q\cdot\bar f')-(f\cdot f')(f\cdot\bar f)(q\cdot\bar q)(\bar q\cdot\bar f')-(f\cdot f')(f\cdot\bar f)(q\cdot\bar f')(\bar q\cdot\bar f)-(f\cdot q)(f\cdot\bar q)(f'\cdot\bar f)(\bar q\cdot\bar f')\ ,\\
T_5&=(f\cdot\bar f)(q\cdot\bar q)(f'\cdot\bar q)(q\cdot\bar f')-(f\cdot q)(\bar q\cdot\bar f)[(f\cdot f')(\bar f\cdot\bar f')+(f'\cdot\bar q)(q\cdot\bar f')]-(f\cdot\bar q)(q\cdot\bar f)[(f\cdot\bar f')(f'\cdot\bar f)+(f'\cdot\bar q)(q\cdot\bar f')]\ ,\\
T_6&=(f\cdot\bar f)[(f\cdot\bar q)(f'\cdot q)(q\cdot\bar f')+(f\cdot\bar q)(f'\cdot\bar f')(q\cdot\bar f)+(f'\cdot\bar q)(q\cdot\bar f)(\bar q\cdot\bar f')]\ ,\\
T_7&=(f\cdot f')(f\cdot\bar f')(q\cdot\bar f)(\bar q\cdot\bar f),\quad \bar T_i=T_i(q\leftrightarrow\bar q, f\leftrightarrow\bar f, f'\leftrightarrow\bar f')\ .
\end{aligned}\tag{E5}$$

Here K and J are the momentum transfer in the $\hat t$ and $\hat u$ channel and are given by

$$K=q-f-\bar f,\quad J=f+\bar f-\bar q\ . \tag{E6}$$

The coefficients A, B, C, D, and E are combinations of the Z-boson–to–fermion couplings. These coefficients can be written

$$\begin{aligned}
A&=A_+B_+C_++A_+B_-C_-+A_-B_+C_-+A_-B_-C_+\ ,\\
B&=A_+B_+C_++A_+B_-C_--A_-B_+C_--A_-B_-C_+\ ,\\
C&=A_+B_+C_+-A_+B_-C_-+A_-B_+C_--A_-B_-C_+\ ,\\
D&=A_+B_+C_+-A_+B_-C_--A_-B_+C_-+A_-B_-C_+\ ,\\
E&=A_+B_+C_+\ ,
\end{aligned}\tag{E7}$$

where

$$\begin{aligned}
A_+&=(g_V^f)^2+(g_A^f)^2,\quad A_-=2g_V^fg_A^f\ ,\\
B_+&=(g_V^{f'})^2+(g_A^{f'})^2,\quad B_-=2g_V^{f'}g_A^{f'}\ ,\\
C_+&=[(g_V^q)^2+(g_A^q)^2]^2+4(g_V^q)^2(g_A^q)^2\ ,\\
C_-&=4g_V^qg_A^q[(g_V^q)^2+(g_A^q)^2]\ .
\end{aligned}\tag{E8}$$

These formulas numerically reproduce the cross section results of Ref. 23 for ZZ production.

APPENDIX F: MATRIX ELEMENT SQUARED FOR WZ PRODUCTION WITH W DECAY

The process considered is

$$d\bar u\to W^-Z,\quad W^-\to l\bar\nu \tag{F1}$$

corresponding to the Feynman diagrams in Fig. 3(c). The traces of gamma matrices were evaluated both by hand and by the algebraic computer program REDUCE. The spin/color-averaged matrix element squared can be written

$$|\mathcal{M}|^2=\tfrac14\langle\tfrac13\rangle\left[\frac{4\pi\alpha}{x_W}\right]^3|U_{ud}|^2|D_W(W)|^2\times(|\mathcal{M}_a|^2+|\mathcal{M}_b|^2+|\mathcal{M}_c|^2+I_{ab}+I_{ac}+I_{bc})\ . \tag{F2}$$

where the $|\mathcal{M}_i|^2$ terms represent the square of a graph and the I_{ij} terms represent the interference between two graphs. These terms can be written

$$\begin{aligned}
|\mathcal{M}_a|^2&=\frac{(g_V^d+g_A^d)^2}{\hat u^2(1-x_W)}F_a\ ,\\
|\mathcal{M}_b|^2&=\frac{(g_V^u+g_A^u)^2}{\hat t^2(1-x_W)}F_a(\hat u\leftrightarrow\hat t,\ d\leftrightarrow\bar u,\ l\leftrightarrow\bar\nu)\ ,\\
|\mathcal{M}_c|^2&=\frac{2(1-x_W)}{(\hat s-M_W^2)^2+(\Gamma_WM_W)^2}F_c\ ,\\
I_{ab}&=-\frac{(g_V^d+g_A^d)(g_V^u+g_A^u)}{\hat u\hat t(1-x_W)}F_{ab}\ ,\\
I_{ac}&=\frac{4(g_V^d+g_A^d)}{\hat u}\frac{(\hat s-M_W^2)}{(\hat s-M_W^2)^2+(\Gamma_WM_W)^2}F_{ac}\ ,\\
I_{bc}&=-I_{ac}(\hat u\leftrightarrow\hat t, d\leftrightarrow\bar u, l\leftrightarrow\bar\nu)\ .
\end{aligned}\tag{F3}$$

The Mandelstam variables are

$$\hat s=(d+\bar u)^2,\quad \hat t=(d-W)^2,\quad \hat u=(d-Z)^2\ , \tag{F4}$$

and the F factors are

$$
\begin{aligned}
F_a &= 2(M_Z^2-\hat{u})(Z\cdot\bar{v})(\bar{u}\cdot l)-(2M_Z^2-\hat{u}^2/M_Z^2)(d\cdot\bar{v})(\bar{u}\cdot l)\ , \\
F_c &= 4\hat{s}[(\bar{u}\cdot l)(Z\cdot\bar{v})+(d\cdot\bar{v})(Z\cdot l)-M_Z^2W^2/4]-W^2(M_Z^2-\hat{u})[(\bar{u}\cdot l)-(\bar{u}\cdot\bar{v})+W^2/2-\hat{u}/2] \\
&\quad -W^2(M_Z^2-\hat{t})[(d\cdot\bar{v})-(d\cdot l)+W^2/2-\hat{t}/2]+2(d\cdot\bar{v})(\bar{u}\cdot l)[(\hat{s}-W^2)^2/M_Z^2-2\hat{s}-2W^2-M_Z^2]+4M_Z^2(\bar{u}\cdot\bar{v})(d\cdot l)\ , \\
F_{ab} &= \hat{s}[(Z\cdot l)(d\cdot\bar{v})+(Z\cdot\bar{v})(\bar{u}\cdot l)-M_Z^2W^2/4-2(\bar{u}\cdot l)(d\cdot\bar{v})]-(M_Z^2-\hat{t})(d\cdot l)(d\cdot\bar{v})-(M_Z^2-\hat{u})(\bar{u}\cdot l)(\bar{u}\cdot\bar{v}) \\
&\quad +(\hat{u}-M_Z^2)(\hat{t}-M_Z^2)(\bar{u}\cdot l)(d\cdot\bar{v})/M_Z^2+M_Z^2(d\cdot l)(\bar{u}\cdot\bar{v})\ , \\
F_{ac} &= -(d\cdot\bar{v})(\bar{u}\cdot l)[\hat{u}(\hat{s}-W^2)/M_Z^2+\hat{s}+W^2+M_Z^2]+(d\cdot\bar{v})(d\cdot l)(\hat{t}-M_Z^2)+(\bar{u}\cdot l)(\hat{u}-M_Z^2)W^2/2 \\
&\quad +(\bar{u}\cdot l)(\bar{v}\cdot Z)(\hat{s}-\hat{u}+M_Z^2)+\hat{s}(Z\cdot l)(d\cdot\bar{v})+M_Z^2(d\cdot l)(\bar{u}\cdot\bar{v})-\hat{s}M_Z^2W^2/4\ ,
\end{aligned}
\tag{F5}
$$

where W denotes the four-momentum of the decaying W boson; $W=l+\bar{v}$. These formulas numerically reproduce the cross-section results of Ref. 24 for WZ production.

[1]V. Barger, H. Baer, A. D. Martin, E. W. N. Glover, and R. J. N. Phillips, Phys. Lett. **133B**, 449 (1983); Phys. Rev. D **29**, 2020 (1984).

[2]D. B. Cline and M. Mohammadi, University of Wisconsin Report No. WISC-EX-86-269, 1986 (unpublished).

[3]UA1 Collaboration, C. Albajar *et al.*, Phys. Lett. B **185**, 241 (1987); also R. Batley, CERN Report No. CERN-EP/86-181, 1986 (unpublished).

[4]V. Barger and R. J. N. Phillips, Phys. Lett. B **189**, 474 (1987).

[5]V. Barger, J. Ohnemus, and R. J. N. Phillips, Phys. Rev. D **35**, 158 (1987).

[6]V. Barger, H. Baer, K. Hagiwara, and R. J. N. Phillips, Phys. Rev. D **30**, 947 (1984).

[7]E. Eichten, I. Hinchliffe, K. Lane, and C. Quigg, Rev. Mod. Phys. **56**, 579 (1984).

[8]V. Barger, T. Gottschalk, J. Ohnemus, and R. J. N. Phillips, Phys. Rev. D **32**, 2950 (1985).

[9]F. Paige and S. Protopopescu, in *Proceedings of the Summer Study on the Physics of the Superconducting Super Collider,* Snowmass, Colorado, 1986, edited by R. Donaldson and J. Marx (Division of Particles and Fields of the APS, New York, 1987), p. 320.

[10]H.-U. Bengtsson and T. Sjöstrand, Report No. UCLA-87-001, 1987 (unpublished) or LU TH 87-3, 1987 (unpublished); in *Proceedings of the Summer Study on the Physics of the Superconducting Super Collider* (Ref. 9), p. 311.

[11]UA1 Collaboration, G. Arnison *et al.*, Phys. Lett. **122B**, 103 (1983); **126B**, 398 (1983); **134B**, 469 (1984); **147B**, 241 (1984).

[12]V. Barger, K. Hagiwara, W.-Y. Keung, and J. Woodside, Phys. Rev. D **31**, 528 (1985).

[13]S. S. D. Willenbrock and D. A. Dicus, Phys. Lett. **156B**, 429 (1985).

[14]K. Hagiwara and D. Zeppenfeld, Nucl. Phys. **B274**, 1 (1986).

[15]W. J. Stirling, R. Kleiss, and S. D. Ellis, Phys. Lett. **163B**, 261 (1985).

[16]J. F. Gunion, Z. Kunszt, and M. Soldate, Phys. Lett. **163B**, 389 (1985).

[17]D. Froidevaux (private communication); Proceedings of La Thuile Workshop on Physics at Future Accelerators, La Thuile, Italy, 1987 (unpublished).

[18]S. Dawson *et al.*, in *Proceedings of the Summer Study on the Design and Utilization of the Superconducting Super Collider,* Snowmass, Colorado, 1984, edited by R. Donaldson and J. Morfin (Division of Particles and Fields of the APS, New York, 1985), p. 263.

[19]K. Hagiwara, R. D. Peccei, D. Zeppenfeld, and K. Hikasa, Nucl. Phys. **B282**, 253 (1987).

[20]T. Gottschalk, in *Proceedings of the UCLA Workshop on Monte Carlo Simulation and Detector Capabilities,* Los Angeles, California, 1986, edited by H.-U. Bengtsson, C. Buchanan, T. Gottschalk, and A. Soni (World Scientific, Singapore, 1986), p. 362.

[21]V. Barger, J. Ohnemus, and R. J. N. Phillips, Phys. Rev. D **35**, 166 (1987).

[22]H. Baer, V. Barger, and R. J. N. Phillips, Phys. Rev. D **32**, 688 (1985).

[23]R. W. Brown and K. O. Mikaelian, Phys. Rev. D **19**, 922 (1979).

[24]R. W. Brown, D. Sahdev, and K. O. Mikaelian, Phys. Rev. D **20**, 1164 (1979).